Couhert, A., Mercier, F., Moyard, J., Biancale, R. (2018): Systematic Error Mitigation in DORIS-Derived Geocenter Motion. - *Journal of Geophysical Research*, *123*, 11, pp. 10,142—10,161.

DOI: http://doi.org/10.1029/2018JB015453

Journal of Geophysical Research: Solid Earth

RESEARCH ARTICLE
10.1029/2018JB015453

Systematic Error Mitigation in DORIS-Derived Geocenter Motion

Alexandre Couhert[1], **Flavien Mercier**[1], **John Moyard**[1], **and Richard Biancale**[2,3]

[1]Centre National d'Etudes Spatiales, Toulouse, France, [2]Deutsche GeoForschungsZentrum, Oberpfaffenhofen, Germany, [3]Groupe de Recherche de Géodésie Spatiale, Toulouse, France

Abstract Geocenter motion observation is one of the most demanding applications of high-precision geodetic techniques. Here a quantitative framework is derived that shows how dominant sources of correlations and modeling issues should be mitigated when estimating the geocenter coordinates. While obtaining independent Doppler Orbitography and Radiopositioning Integrated by Satellite-based geocenter time series, this paper shows how DORIS data and the Ocean Surface Topography Mission (OSTM)/Jason-2 satellite can contribute to allow insight into model and geodetic technique errors and provide an independent assessment of the ITRF2014 origin stability: In particular, about ∼ 5mm offset along the X axis and ∼ 2mm higher annual amplitude in the axial direction were estimated for the geocenter coordinates over the period 2008.5–2015.5. To first order, Yarkovsky-Schach coupling mutes Satellite Laser Ranging (SLR) + Laser Geodynamics Satellite (LAGEOS) geocenter solutions, when station heights and biases are adjusted to mitigate their modeling errors.

Key Points:
- Independent geocenter coordinates were derived using DORIS data and the OSTM/Jason-2 satellite
- Sources of correlations and modeling issues were identified and mitigated
- Uncertainties in the realization of the ITRF origin are addressed

Correspondence to:
A. Couhert,
alexandre.couhert@cnes.fr

Citation:
Couhert, A., Mercier, F., Moyard, J., & Biancale, R. (2018). Systematic error mitigation in DORIS-derived geocenter motion. *Journal of Geophysical Research: Solid Earth*, *123*, 10,142–10,161. https://doi.org/10.1029/2018JB015453

Received 10 JAN 2018
Accepted 15 OCT 2018
Accepted article online 19 OCT 2018
Published online 8 NOV 2018

1. Introduction

Nontidal mass redistribution in the Earth's fluid envelope (atmosphere, oceans, continental water, and ice sheets) plays an essential role in the dynamics of the whole planet's gravity field, rotation, and center of mass motion relative to a crust-fixed reference frame (or geocenter). In particular, major mass redistribution directly reflects in the nontidal geocenter motion and dominates at seasonal variations (Dong et al., 1997). Since a consensus model for the nontidal component of the geocenter motion is not part of the current IERS Conventions 2010 (Petit & Luzum, 2010), it is therefore imperative to understand its driving mechanisms.

As noted by Collilieux et al. (2009), different definitions for the term "geocenter motion" exist in the literature (expression, sign, and method of realization). The diversity of conventions proposed reflects the uncertainty surrounding its rigorous treatment. Following the conventions in Ray (1999), we consider the motion of the center-of-mass (CM) of the whole Earth with respect to the center-of-figure (CF) of the solid Earth surface, that is, the geometrical center of the Earth's surface. The IERS Conventions 2010 substitute the International Terrestrial Reference Frame (ITRF) origin for CF, approximately located with a fixed offset from CF (Wu et al., 2012). Because satellites dynamical motion defines CM, about which they orbit (according to Newton's laws), and ground station networks are located on the solid Earth surface, satellite geodetic techniques have been primarily used to determine geocenter motion.

In practice, geodetic networks coverage of the Earth surface is limited, hence CF remains a purely theoretical concept. Instead, only their center-of-network (CN) is accessible, contributing to apparent geocenter motion and giving rise to "network effects" (Tregoning & van Dam, 2005; Zannat & Tregoning, 2017). This complicates a direct comparison of the different tracking technique geocenter estimates. Among the space geodetic techniques, Satellite Laser Ranging (SLR) is currently the only one which derives well-established geocenter coordinates (Sośnica, 2015; Wu et al., 2012) and defines solely the origin of ITRF2014 (Altamimi et al., 2016). The geocenter vector measured by Doppler Orbitography and Radiopositioning Integrated by Satellite (DORIS) has been determined with a lesser precision (especially for the Z component) (Willis et al., 2006), as was to be expected given the less accurate positioning information, and the significant challenges to precise orbit determination (modeling of the nongravitational forces) presented by the satellites tracked. However, unlike SLR whose operational stations are sparse and not permanently available (i.e., resulting in a "time-varying" configuration of the network), the DORIS (and Global Navigation Satellite System, GNSS) tracking network is more stable and uniquely well distributed geographically. Therefore, DORIS-derived geocenter motion may

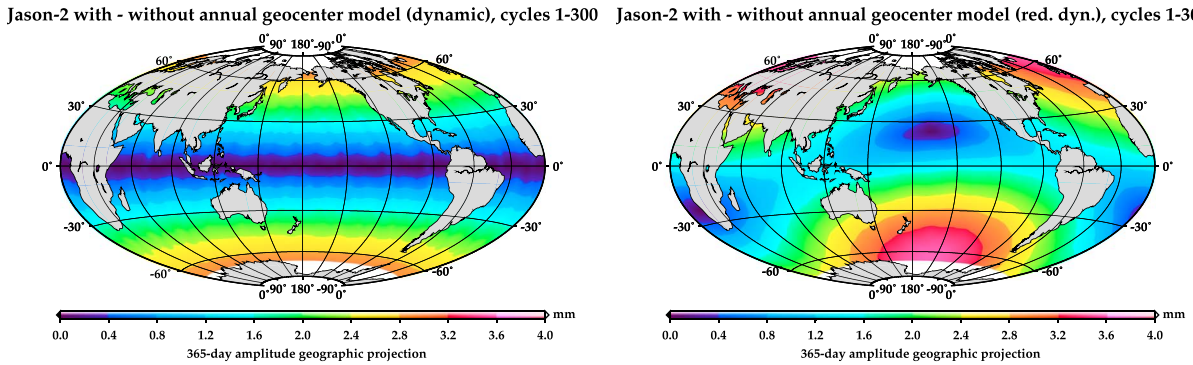

Figure 1. Jason-2 geographically correlated radial difference 365-day signals (cycles 1–300; July 2008–August 2016), between DORIS-only orbit series including or not the SLR-derived Ries annual geocenter model, for dynamic (left) and reduced-dynamic (right) solutions, over 3.5° × 3.5° bins. SLR = Satellite Laser Ranging; DORIS = Doppler Orbitography and Radiopositioning Integrated by Satellite.

prove better referenced to CF. Likewise, as a microwave tracking system, DORIS observations are not limited to cloudless weather, which can adversely create systematic effects in SLR-based estimations. Riddell et al. (2016) outlined the importance of providing independent geocenter time series to allow insight into model and geodetic technique errors. To this end, DORIS could significantly contribute to future realizations of the ITRF origin.

Analyzing the principal sources of long-term errors (annual to decadal time scales) affecting satellite altimetry orbit time series at regional scales, Couhert et al. (2015) identified the nontidal geocenter motion as the largest limiting factor when comparing orbits based on different tracking techniques (GNSS, DORIS, and SLR). Blewitt (2003) and Wu et al. (2012) also stressed a need for improved knowledge of how errors in the geocenter location map into station and tide gauge measurements (which are used to calibrate and validate altimeter errors) when determining regional mean sea level (MSL) changes. Furthermore, the transfer function to the orbit (then aliased directly into any calculation of MSL) is rather complex: Depending on the parameterization (as well as the tracking measurement) used, only Z (north-south direction) systematic errors will propagate into the orbit estimation and derived MSL (Beckley et al., 2007; Morel & Willis, 2005), due to canceling effects from the Earth's rotation in dynamic orbits. This is illustrated in Figure 1, which shows the exclusive north-south impact of including a seasonal (annual) model (SLR-derived from Ries, 2013) of Earth geocenter variations in dynamic orbits (Figure 1, left), as opposed to reduced dynamic solutions (Figure 1, right), exhibiting additional contaminations in the east-west direction.

If significant seasonal variations appear in all three components of the geocenter motion (Cheng et al., 2013; Crétaux et al., 2002), with regional geocentric sea level rates primarily affected by any ITRF origin drift error, annual geocenter models may not be sufficiently precise for accurate determination of MSL rise. Therefore, it is important to monitor and model the nonlinearity of geocenter motion (Dong et al., 2014), especially as this issue remains insufficiently addressed (Lavallée et al., 2006).

Here we use Ocean Surface Topography Mission (OSTM)/Jason-2 DORIS-only solutions to (i) prove that DORIS has the sensitivity to monitor geocenter motion; (ii) analyze which processes are responsible for the corruption of DORIS-based geocenter estimates; and (iii) assess the validity of the obtained geocenter time series through comparisons to independent estimations. Section 2 introduces the theoretical framework of our analysis, regarding rigorously determined geocenter motion. Section 3 describes the data sources and processing methods. Section 4 analyzes the relative importance of different processes to be mitigated, when solving for geocenter coordinates using DORIS or SLR observations, as well as comparisons to independent estimates. Thus, uncertainties in the realization of the ITRF origin can be disentangled. Section 5 summarizes the conclusions.

2. Theoretical Framework

2.1. Methods for Determining Geocenter Motion

Different methods have been used for geocenter motion determination. The *dynamic* approach, solving for the degree-one coefficients of the geopotential, is equivalent to the *kinematic* approach, which directly estimates the net translational offsets of the network. In the *geometric* or *network shift* (Dong et al., 2003)

approach, a free-network solution in a CM frame is first obtained (as in Heflin et al., 1992), before determining the three translation parameters via seven- or six-parameter (three translations, three rotation angles, and sometimes a scale parameter) similarity transformations. From a crust-fixed (CE—CM of the solid Earth—or CF) reference frame, a degree-one mass load on the Earth's crust does not manifest as an observable translation (CM frame), but as a degree-one deformation in the network (Blewitt, 2003). *Inverse* determinations (e.g., the *degree-1 deformation* approach, Blewitt et al., 2001, or the *CM method*, Lavallée et al., 2006) generally use a set of globally distributed Global Positioning System (GPS) stations to observe geocenter motion through this deformation signal—a primary exception being the *GRACE-OBP* approach (Sun et al., 2017; Swenson et al., 2008), which only combines data from the Gravity Recovery and Climate Experiment (GRACE) satellite mission and the output of an Ocean Bottom Pressure (OBP) model; it contains less seasonal signal than direct satellite estimates, while being subject to unknown errors in the OBP model used (in this respect, Chanard et al. (2018) proposed a promising approach without relying on OBP models and obtained larger annual amplitudes for the Z geocenter component than past results). However, there are reasons to be skeptical of the present inversions that use GPS data, since only about 50% of the vertical GPS signal and about 10% in the horizontal signal are caused by unmodeled geophysical loading. The rest comes from other effects, and in particular harmonics of the GPS draconitic frequency (1.04 cycle per year) are considerably larger than annual loads in the North/East directions and about 2/3 the size of the annual vertical loads (Ray et al., 2008). The *unified* approach of Wu et al. (2017) artificially extends the SLR network through the use of co-motion constraints, though their use remains to be clarified given the usual poor level of agreement between colocated geodetic station time series. Thus, we focus here on the kinematic and network shift approaches.

2.2. Network Solutions

To solve for satellite orbits and station positions using DORIS observations, it is necessary to fix the inertial orientation (e.g., the Geocentric Celestial Reference Frame [GCRF] for the Earth) and the position of the Earth in this coordinate system. An Earth-orbiting satellite's motion is modeled in this frame. The station coordinates are expressed in the ITRF, based on the IERS models (Petit & Luzum, 2010). Hence, these coordinates can represent a geocenter motion (global translation of all stations expressed in the Earth's reference frame), and rotations around the X and Y axes (polar motion), or the Z axis. The global translations in the X and Y directions (i.e., in the equatorial plane) and rotations around the X and Y axes are well observed thanks to the Earth's rotation, which is modeled over the time span of the measurements. For the Z (north-south) translation, it can be observed thanks to the satellite dynamics and a consistent choice of empirical accelerations. For the rotation characteristics around the Z axis, the once-per-revolution (OPR) empirical terms in the normal direction prevent observation of the length of day (which is therefore not adjusted), and the unknown satellite initial state vectors (orbital plane orientation) prevent observation of the rotation bias of the network around the Z axis. As a consequence, using DORIS data and the current parameterization only allow the observation of translations in the X, Y, and Z directions, and rotations around the X and Y axes. That is, a solution for the network will have a rank-1 deficiency due to the unobservable rotation around the Z axis.

2.2.1. Normal Equations for a Network Solution

To achieve a network solution using measurements between ground stations and satellites, the measurement model equations are linearized around a reference solution. The reference solution is chosen in order to stay in the domain where the linearization is valid (e.g., the current ITRF coordinates can be used). The complete parameterization uses the satellite dynamic parameters (e.g., initial positions and velocities, and empirical accelerations), measurement parameters (e.g., troposphere delays), and station coordinates. After reduction on the set of stations coordinates, the solution is written as a least squares minimization problem

$$J(x) = x^t Q x - 2x^t B + J_0, \tag{1}$$

where x is a column vector of the station coordinate variations relative to the reference solution (three values for each station); Q is a symmetric positive matrix (obtained from the partial derivatives of the measurements relative to the model parameters after reduction); B are the corresponding residuals; and J_0 is the least squares criterion corresponding to $x = 0$ (norm of the residuals for the reference solution). The network shift solution is found by minimizing $J(x)$ with respect to x. The symmetric matrix Q is positive and nearly singular (rank-1 deficiency, as explained above).

2.2.2. Kinematic and Network Shift Approaches

The objective here is to analyze the common motion of the network (three translations and three rotations). They are represented by a matrix A. Each column corresponds to the elementary rigid displacements of the

network (translations and rotations around the frame axes). The corresponding network displacements are $x = Ay$, with y the six-component vector of translations and rotations. A is a six-column matrix, whose rank is six. The six parameters contained in y can be estimated using two methods:

1. Kinematic: y is directly estimated from equation (1) and the expression of the station coordinates $x = Ay$. The solution y_{ki} minimizes $y^t \left(A^t Q A\right) y - 2y^t \left(A^t B\right) + J_0$.
2. Network shift: The parameters of y are adjusted on a known network solution defined by the normal equations (x_0, P_{x_0}), where x_0 is the vector of station coordinate variations relative to the chosen reference and P_{x_0} the corresponding covariance matrix (symmetric positive). The six transformation parameters of y_{ns} minimize the quadratic criterion $\left(Ay - x_0\right)^t P_{x_0}^{-1} \left(Ay - x_0\right)$.

If the matrix Q in equation (1) is positive definite, the kinematic solution y_{ki} and the network shift solution y_{ns} are identical (in this case $P_{x_0} = Q^{-1}$).

Unfortunately if the measurements are only between the Earth and satellites (just as in the case of the DORIS geodetic technique), the rotation around the Z axis is not observable and the matrix Q is singular. This is usually handled in the network shift approach using a set of arbitrary loose constraints applied on the coordinate variations x, in order to obtain non singular matrixes. For example the constraints can be applied directly on the three station coordinates (i.e., diagonal constraints). This approach results in adding to Q a diagonal matrix D with small diagonal terms ($1/\sigma^2$ with σ associated to the constraint, e.g., 1 m). In this case $P_{x_0} = (Q + D)^{-1}$ and $x_0 = (Q + D)^{-1} B$. If we consider the constraints as a set of measurements, the constrained solutions are identical in both approaches. However, the constraint is only needed to define normal equations for the network shift solution. To compare the kinematic with the network shift approach in the case of loose constraints, we have to compare the solutions minimizing the following criteria

$$J(x) = y^t \left(A^t Q A\right) y - 2y^t \left(A^t B\right) + c, \tag{2}$$

for the exact kinematic solution, y_{ki}, and

$$\begin{aligned} J(x) &= \left(Ay - x_0\right)^t (Q + D) \left(Ay - x_0\right), \\ &= y^t \left(A^t (Q + D) A\right) y - 2y^t \left(A^t B\right) + x_0^t (Q + D) x_0, \end{aligned} \tag{3}$$

for the constrained network shift solution, y_{ns}.

Due to the structure of Q, $A^t Q A$ has a structure with a 5×5 upper left block of full rank, and zeros (or very small terms due to numerical errors) in the sixth row and column. We find an indetermination in the kinematic solution: the criterion has no minimum if the sixth row of $A^t B$ is not null, which is usually the case due to the contributions of measurement errors. So only translations along the X, Y, and Z directions, and rotations around the X and Y axes can be estimated. The Z rotation cannot be determined, as expected. By expressing the problem on the two subspaces defined with the first five terms of y (subscript $_1$) and the last term of y (subscript $_2$), the matrixes for the second criterion have the following structure

$$\begin{aligned} A^t (Q + D) A &= \begin{bmatrix} Q_{11} + D_{11} & D_{12} \\ D_{21} & D_{22} \end{bmatrix} \\ A^t B &= \begin{bmatrix} B_1 \\ B_2 \end{bmatrix}, \end{aligned} \tag{4}$$

and the solution on the five-observable transformation is given by

$$\left(Q_{11} + D_{11} - D_{12} D_{22}^{-1} D_{21}\right) y_1 = B_1 - D_{12} D_{22}^{-1} B_2. \tag{5}$$

This last expression is very interesting as the terms from the matrix D vanish on the left-hand side when D approaches zero. Conversely, on the right-hand side, the term $D_{12} D_{22}^{-1} B_2$ generates a bias. For example, if D is proportional to ϵ and ϵ approaches zero, this term becomes constant. As such, it has to be minimized if the network shift approach is used without removing loose constraints; see Davies and Blewitt (2000) for further discussion. When the network is homogeneous, the term D_{12} is small provided D is proportional to the identity matrix, as the different rigid transformations are almost orthogonal. It is also possible to choose the matrix D

Table 1
Effect of Adjusting Station Heights on the Annual Components of the Geocenter Motion of the DORIS-Derived Geocenter Motion From Jason-2

Solution	*A* ratio	$\delta\phi$ (day)
Height adjustment		
DX	1.7	−82
DY	1.1	1
DZ	0.4	−9

Note. *A* ratio = amplitude ratio; $\delta\phi$ = phase shift; DORIS = Doppler Orbitography and Radiopositioning Integrated by Satellite.

in order to have D_{12} equal to zero, as the different contributions to D can be modeled correctly (e.g., $D = \epsilon CC^t$ with C a column orthogonal to the first five columns of A).

As a consequence, in the rest of the study, we rely on kinematic solutions, which are identical to network shift solutions if constraints are correctly handled. Owing to the dense and well-distributed network of DORIS stations, rotations are sufficiently orthogonal to translations (when constraints are *minimal*) so that in this work we only consider the latter (i.e., rotations are not adjusted) for DORIS-based kinematic estimates of geocenter motion.

2.3. Station Height Inaccuracy

As suggested in Rothacher (2002), station heights will always be less accurate than their horizontal positions. Indeed, the error sources affecting the station height estimation are manifold: Nontidal (atmospheric, hydrological) loading corrections are currently mismodeled (whose associated surface displacements are the largest for the vertical component), multipath and DORIS Ultra Stable Oscillator (USO) frequency variations reduce the quality of the height estimates, and above all the troposphere delay parameters are correlated with the station height. Accordingly, if not taken into account, the Zenith Tropospheric Delay (ZTD) estimates will absorb most of these errors and g et aliased while determining geocenter motion. To mitigate this effect, the station heights are estimated simultaneously with the geocenter translation, orbit, force and DORIS measurement parameters in our kinematic *unconstrained* solutions (with no a priori uncertainty). The geocenter coordinates determined with heights adjusted instead of holding fixed station positions are diversely affected, as can be seen in Table 1 by the substantial negative X phase shift, as well as the larger and lower amplitudes of the X and Z annual components, respectively. Part of the differences observed in the Z direction may also have to do with the collinearity issue of the estimated T_Z geocenter coordinate with the residual OPR perturbations Jason-2 modeling errors in the radial direction (R_{s_0}) unveiled in section 4.2.

Since individual vertical site displacements $\left(\Delta\vec{r}^{\,\mathrm{CF}}_{i,\mathrm{load}_{\mathrm{nontidal}}}\right)$ are thus estimated for the whole network of stations, the effect of unmodeled station nontidal deformations (especially soil moisture, groundwater, snow, and ice) on the nontidal geocenter solutions $\left(\vec{O}_{\mathrm{G}_{\mathrm{nontidal}}}\right)$ is lowered. Following our analysis, the coordinates of a site i in the CM reference frame ($\vec{X}^{\mathrm{CM}}_i$) can be written as

$$\vec{X}^{\mathrm{CM}}_i(t) \simeq \vec{X}^{\mathrm{CN}}_{i,\mathrm{ITRF}}(t_0) + (t - t_0)\dot{\vec{X}}_{i,\mathrm{ITRF}} + \Delta\vec{c}^{\,\mathrm{CM}}_{i,\mathrm{load}_{\mathrm{tidal}}}(t) + \Delta\vec{r}^{\,\mathrm{CF}}_{i,\mathrm{load}_{\mathrm{nontidal}}}(t) - \vec{O}_{\mathrm{G}_{\mathrm{nontidal}}}(t), \tag{6}$$

where $\vec{X}^{\mathrm{CN}}_{i,\mathrm{ITRF}}(t_0)$ is the ITRF coordinates of station i at a reference epoch t_0; $\dot{\vec{X}}_{i,\mathrm{ITRF}}$ is its associated linear velocity vector; $\Delta\vec{c}^{\,\mathrm{CM}}_{i,\mathrm{load}_{\mathrm{tidal}}}(t)$ and $\Delta\vec{r}^{\,\mathrm{CF}}_{i,\mathrm{load}_{\mathrm{nontidal}}}(t)$ are the site i surface displacements correction in the CM frame from tidal loading models and nontidal radial deformation adjusted in the CF frame, respectively. $\Delta\vec{r}^{\,\mathrm{CF}}_{i,\mathrm{load}_{\mathrm{nontidal}}}(t)$ and $\vec{O}_{\mathrm{G}_{\mathrm{nontidal}}}(t)$ can be considered constant over typical arc lengths of a few days, as annual variations dominate in both time series. Overall, this leads to better sense the motion of CF relative to CM (because CF is only measurable from motions of crust-fixed stations), while the traditional translational approaches (dynamic, kinematic, and network shift) rather observe the variation of CN with respect to CM, as they do not account for the station network nontidal deformations when determining the geocenter trajectory.

3. Data and Processing Methods

The latest release of precise orbit ephemerides (POE) on the Jason-2 series Geophysical Data Records (GDR), computed by the Centre National d'Etudes Spatiales (CNES), are referred to as version "E" (see Dumont et al., 2017, available at https://www.aviso.altimetry.fr/fileadmin/documents/data/tools/hdbk_j2.pdf, or Stammer & Cazenave, 2018, for details about the GDR-E orbit standards). The background models employed in the GDR-E solutions are consistent with the IERS 2010 conventions. The DORIS station coordinates are based on DPOD2008 complementing the ITRF2008 (Altamimi et al., 2011) with some additional stations and coordinate updates. The modeled station displacements are restricted to tidal loading signals, with their induced geocenter variations. In the context of this study, the SLR-derived Ries annual (nontidal) geocenter model was not applied here, contrary to the GDR-E-like dynamic orbit solutions.

Residual dynamic modeling errors are accommodated in 10-day (the orbit's repeat cycle) arcs, over 7 years from July 2008 to June 2015, by the adjustment of one drag coefficient per arc, daily cross-track/along-track

Table 2
Effect of Incorporating Low-Elevation Data on the Annual Components of the Geocenter Motion of the DORIS-Derived Geocenter Motion From Jason-2

Solution	*A* ratio	$\delta\phi$ (day)
Low elevations		
DX	0.7	17
DY	0.9	1
DZ	5.2	39

Note. *A* ratio = amplitude ratio; $\delta\phi$ = phase shift; DORIS = Doppler Orbitography and Radiopositioning Integrated by Satellite.

OPR accelerations, and empirical along-track constant accelerations estimated for every two orbital revolutions. For the DORIS measurement parameterization, range-rate biases are solved for per pass, alongside troposphere wet biases. As mentioned in section 2, the station heights and the geocenter translation are adjusted per arc besides.

Due to correlations between the ZTD and the station heights, the choice of tropospheric modeling strategy can influence the retrieval of precise geocenter coordinates from space geodetic microwave techniques such as DORIS. The Vienna Mapping Function 1 (VMF1; Boehm, Werl, & Schuh, 2006) and zenith hydrostatic delays (ZHDs) derived from the European Centre for Medium-Range Weather Forecasts (ECMWF) numerical weather models (NWMs) are the best modeling approach currently available. Unfortunately, the site-dependent VMF1 time series are not available globally for all epochs since 1994 for the following sites: Ajaccio, France; Betio, Kiribati; Cold-Bay, USA; Dionysos, Greece; Grasse, France; Le-Lamentin, France (Caribbean Islands); Male, Maldives; Miami, USA; Monument-Peak, USA; Owenga, New-Zealand; Paramashir, Russia; Rikitea, France (Polynesia), and Santa-Cruz, Ecuador. Thus, the necessary exclusion of the aforementioned DORIS stations happens to be more harmful to geocenter determination (since suffering from a pronounced network effect) than the improvement represented by the VMF1/ECMWF model over the empirical Global Mapping Function (GMF; Boehm, Niell, et al., 2006) and the Global Pressure and Temperature (GPT; Boehm et al., 2007) model used for the computation of the ZHD in the GDR-E orbit standards.

4. Results

To improve our understanding of the current limiting error sources in DORIS-based estimates of geocenter motion, it is important to identify the various processes that may play a role and to do so in a way that exhibits their respective effect on the geocenter coordinates.

4.1. Low-Elevation Data

If station heights have to be adjusted to prevent unrealistic ZTD values — since both are correlated — from corrupting the determination of geocenter motion (as discussed further in section 2.3), one should try to reduce this collinearity issue in order to derive accurate estimates of the vertical station position corrections. That is, we should process DORIS data down to as low elevation angles as possible (from 10° to 5° elevation cut-off angle, corresponding to an increase in the number of observations by up to $\sim$ 20$\c{p}ercnt$;) to better discriminate between height and troposphere parameters (as stated in Böhm et al., 2002, for GNSS and VLBI data). A major limitation of low-elevation measurements is that they are more subject to high noise levels, multipath perturbations, and antenna phase center variations systematic effects, than high elevation data. Therefore, an elevation-dependent weighting of the observations was used, based on DORIS antenna gain and propagation knowledge. Horizontal tropospheric gradients were also solved for per arc to account for the more pronounced azimuthal asymmetries of the troposphere delay at low elevation at seasonal and inter-annual climatic time scale. This is illustrated in Table 2, which shows the asset of using an elevation cut-off angle of 5° instead of 10° (with supplementary adjustment of horizontal tropospheric gradients while down-weighting low-elevation data) to avoid the annual variation of the axial geocenter motion to be more contaminated with noise (see the larger amplitude of the Z annual component).

4.2. Draconitic Effects

If microwave techniques (e.g., DORIS, GNSS) now exhibit equatorial (X, Y) geocenter coordinate estimates comparable to SLR observations, more scatter is still present between the different time series along the spin (Z) axis (Altamimi et al., 2016; Haines et al., 2015). Mismodeling issues, such as Solar Radiation Pressure (SRP), likely are limitations that affect DORIS and GNSS Z geocenter, due to the complex shape of their satellites. Spurious signatures linked to the satellite beta (or draconitic) period ($\sim$ 365-day for DORIS sun-synchronous, $\sim$ 352-day for GPS, and $\sim$ 118 days for the Jason altimetry satellites) are well-known manifestations of such deficiencies and have prompted efforts to reduce these periodic errors. Gobinddass, Willis, de Viron, Sibthorpe, Zelensky, Ries, Ferland, Bar-Sever, Diament,(2009), Gobinddass, Willis, de Viron, Sibthorpe, Zelensky, Ries, Ferland, Bar-Sever, Diament, Lemoine, (2009) considered the reestimation (and then fixing) of DORIS satellites SRP coefficients (C_r) based on long-term data analysis, instead of estimating arc dependent val-

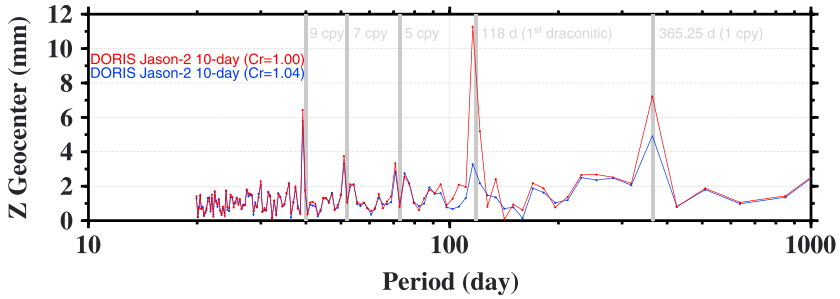

Figure 2. Amplitude spectra of the Z geocenter coordinate obtained using the Lomb-Scargle method for the 10-day estimates of DORIS-derived geocenter motion from Jason-2 GDR-E-like dynamic orbit series (July 2008–June 2015; cycles 1–257), with a SRP coefficient of 1.00 (red) and 1.04 (blue). The vertical lines mark the first draconitic frequency of Jason-2 and integer multiples of the annual frequency. DORIS = Doppler Orbitography and Radiopositioning Integrated by Satellite; SRP = solar radiation pressure; GDR = Geophysical Data Records.

ues. Haines et al. (2015) focused on supplementing data from the terrestrial network with observations from Low-Earth Orbit (LEO) satellite (GRACE) GPS receivers. In both approaches, the draconitic and annual signals could not be well separated and were still aliasing in the Z geocenter estimates.

Willis et al. (2006) and Meindl et al. (2013) outlined the effect of a geocenter Z-shift on the orbital plane; however the impact of a north-south network offset perturbation on satellite dynamics can be clearly explained in the local orbital frame, for low-eccentricity orbits, by the *Hill-Clohessy-Whiltshire equations*

$$\begin{aligned}\ddot{\delta}_R(t) &= 3\omega_0^2\delta_R(t) + 2\omega_0\dot{\delta}_S(t) + P_R(t)\\ \ddot{\delta}_S(t) &= -2\omega_0\dot{\delta}_R(t) + P_S(t)\\ \ddot{\delta}_W(t) &= -\omega_0^2\delta_W(t) + P_W(t),\end{aligned} \tag{7}$$

where the subscripts R, S, and W, denote the radial, along-track and cross-track coordinates, respectively; ω_0 is the uniform angular velocity of the satellite; (P_R, P_S, P_W) and $(\delta_R, \delta_S, \delta_W)$ are the perturbing accelerations and induced orbit perturbations in the co-rotating satellite frame. Assuming the orbital motion is only perturbed by a solved for T_Z-geocenter offset, the usual OPR accelerations in the radial (R_{c_0}, R_{s_0}), along-track (S_{c_0}, S_{s_0}) and cross-track (W_{c_0}, W_{s_0}) directions—which are partially absorbed by the adjusted empirical acceleration parameters (S_c, S_s) and (W_c, W_s)—plus a cross-track bias modeling error C_{N_0}, the perturbing acceleration

$$\begin{aligned}P_R(t) &= -2T_Z\frac{GM}{r^3}\sin i\sin\omega_0 t + R_{c_0}\cos\omega_0 t + R_{s_0}\sin\omega_0 t\\ P_S(t) &= T_Z\frac{GM}{r^3}\sin i\cos\omega_0 t + \left(S_c + S_{c_0}\right)\cos\omega_0 t + \left(S_s + S_{s_0}\right)\sin\omega_0 t\\ P_W(t) &= T_Z\frac{GM}{r^3}\cos i + \left(W_c + W_{c_0}\right)\cos\omega_0 t + \left(W_s + W_{s_0}\right)\sin\omega_0 t + C_{N_0}\end{aligned} \tag{8}$$

consists of contributions in all three directions (with inclination i of the orbit w.r.t. the equatorial plane) owing to the T_Z (e.g., Meindl et al., 2013) and OPR terms. Incorporating this perturbation on the right-hand side of the Hill's equation 7 gives the following complete solution, once drift terms have been canceled out through the adjustment of empirical along-track and cross-track acceleration parameters (S_c, S_s) and (W_c, W_s)

$$\begin{aligned}\delta_R(t) &= -\frac{\dot{\delta}_S(0)}{2\omega_0}\cos\omega_0 t + \frac{\dot{\delta}_R(0)}{\omega_0}\sin\omega_0 t\\ \delta_S(t) &= \left(\frac{1}{{\omega_0}^2}\left[\frac{R_{s_0}}{2} - T_Z\frac{GM}{r^3}\sin i\right] + 2\frac{\dot{\delta}_R(0)}{\omega_0}\right)\cos\omega_0 t\\ &\quad + \left(-\frac{R_{c_0}}{2{\omega_0}^2} + \frac{\dot{\delta}_S(0)}{\omega_0}\right)\sin\omega_0 t - 2\frac{\dot{\delta}_R(0)}{\omega_0} + \delta_S(0)\\ \delta_W(t) &= \delta_W(0)\cos\omega_0 t + \frac{\dot{\delta}_W(0)}{\omega_0}\sin\omega_0 t + \frac{1}{{\omega_0}^2}\left(C_{N_0} + T_Z\frac{GM}{r^3}\cos i\right).\end{aligned} \tag{9}$$

When the tracking system has no observability in the radial direction, the cosine coefficient of the induced orbit perturbation in the along-track direction can be set to zero, owing to the adjustment of the initial radial

Table 3
Effect of Solar Radiation Pressure Tuning on the Annual Components of the Geocenter Motion of the DORIS-Derived Geocenter Motion From Jason-2

Solution	*A* ratio	$\delta\phi$ (day)
Draconitic		
DX	0.9	5
DY	1.0	−2
DZ	0.7	6

Note. *A* ratio = amplitude ratio; $\delta\phi$ = phase shift; DORIS = Doppler Orbitography and Radiopositioning Integrated by Satellite.

velocity (whatever the final value of the solved for T_Z term). This ensures a solely cross-track observability of the Z geocenter motion. Such is the case for DORIS when individual vertical site displacements are estimated (subsection 2.3), and this finding further advocates for adjusting station heights. Because of the stronger tie to the reference network origin of the SLR satellite geodetic technique, range biases for all tracking stations should also be estimated. Otherwise the estimated T_Z geocenter coordinate would end up with an erroneous value, due to the inconsistency between the along-track and cross-track observability of the Z geocenter vector component (the sine, cosine and constant coefficients of the induced orbit perturbation in the radial, along-track and cross-track directions, respectively, cannot be simultaneously nullified since only T_Z and $\dot{\delta}_R(0)$ are adjusted).

Once having secured the exclusive cross-track observability of the Z geocenter motion, the strong collinearity of this component with cross-track bias modeling errors (e.g., SRP) becomes evident

$$T_Z \simeq \frac{-C_{N_0} r^3}{GM \cos i}. \tag{10}$$

The results so far indicate that the SRP modeling errors acting as constant cross-track accelerations, over each of the time intervals composing an arc, should be minimized to prevent draconitic signal from modulating geocenter motion signal along the Z axis. This finding makes clear that sun-synchronous missions, with orbital inclinations close to 90°, are the least favorable for the observability of the Z geocenter coordinate. Indeed, the correlation between T_Z and C_{N_0} is at its highest level in that case, as the denominator of Equation (10) is proportional to the cosine of the inclination angle.

Figure 2 shows the spectral analysis of the Z geocenter component. The amplitude of period related to the first draconitic of Jason-2 (∼ 118 days) is prevalent with the standard SRP coefficient value of 1.00, and can be reduced from 12 to 3 mm when tuning the SRP coefficient to 1.04 (and even less than 1.5 mm in the final solution). That is, aliasing of Jason-2 draconitic error into the Z geocenter coordinate—which manifests also in its annual peak (Table 3)—has been taken care of, through the attenuation of the spurious spectral peak at 118 days in the amplitude of the Z geocenter coordinate. The visible odd overtones of the annual period (harmonics of 5 cycles per year (cpy) up to 9 cpy) indicate that the seasonal cycle cannot be represented by a simple sinusoidal function.

4.3. Lumped Harmonics

When tracking data just from one satellite are used, estimates for the geocenter coordinates ($T_X = C_{1,1}, T_Y = S_{1,1}, T_Z = C_{1,0}$) may represent linear combinations of multiple low degree and order coefficients (i.e., *lumped* harmonics), not just the degree one coefficients. That is, residual errors in higher odd-degree order-0 and

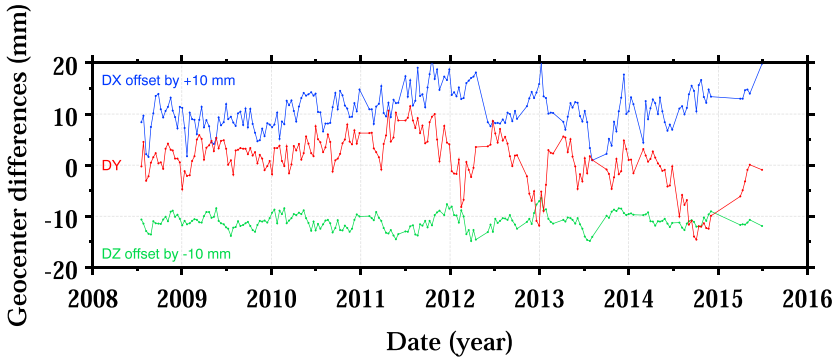

Figure 3. Mean X (blue, offset by +10mm), Y (red), and Z (green, offset by −10 mm) DORIS-derived geocenter coordinate differences per cycle between Jason-2 GDR-E-like solutions (July 2008–June 2015; cycles 1–257), based on the mean gravity field model (with the 6-hr NCEP/AGRA series), and obtained using the monthly gravity field RL05 time series from CSR (with the 3-hr GRACE AOD1B RL05 series). GDR = Geophysical Data Records.

Table 4
Effect of Refining Time-Variable Geopotential Models on the Annual Components of the Geocenter Motion of the DORIS-Derived Geocenter Motion From Jason-2

Solution	*A* ratio	$\delta\phi$ (day)
Geopotential		
DX	2.2	45
DY	0.6	−8
DZ	1.3	2

Note. *A* ratio = amplitude ratio; $\delta\phi$ = phase shift; DORIS = Doppler Orbitography and Radiopositioning Integrated by Satellite.

order-1 terms (e.g., $C_{3,1}, S_{3,1}, C_{3,0}, C_{5,1}, S_{5,1}, C_{5,0}, \ldots$) of the mean gravity field model may reflect in the recovered geocenter time series. To minimize this effect, the monthly series of GRACE-derived gravity field from CSR (RL05), which better represent the instantaneous geopotential than the GDR-E mean gravity field model (extrapolated after 2014.5), are taken as a reference. We have also replaced the GDR-E time-variable atmospheric/oceanic gravitational potential (6-hr NCEP/AGRA series) with the 3-hr GRACE AOD1B RL05 dealiasing products from GFZ, when relying on the monthly GRACE time series.

Figure 3 and Table 4 show the larger equatorial geocenter annual component differences from odd-degree order-1 terms between the GRACE time series and the GDR-E geopotential models. Part of these discrepancies may also originate from lack of accurate modeling of the strong 2011 La Niña and 2014-15 El Niño events in the gravity field model. The apparent noise at shorter time intervals between the two geocenter motion estimates has to do with the coarser 6-hr NCEP/AGRA atmospheric gravity series.

4.4. ITRF Residual Errors

Geocenter motion is related to the realization of the ITRF, as its origin and set of station positions and velocities define the CN, with reference to which is observed CM. Zelensky et al. (2018) thoroughly discussed the impact

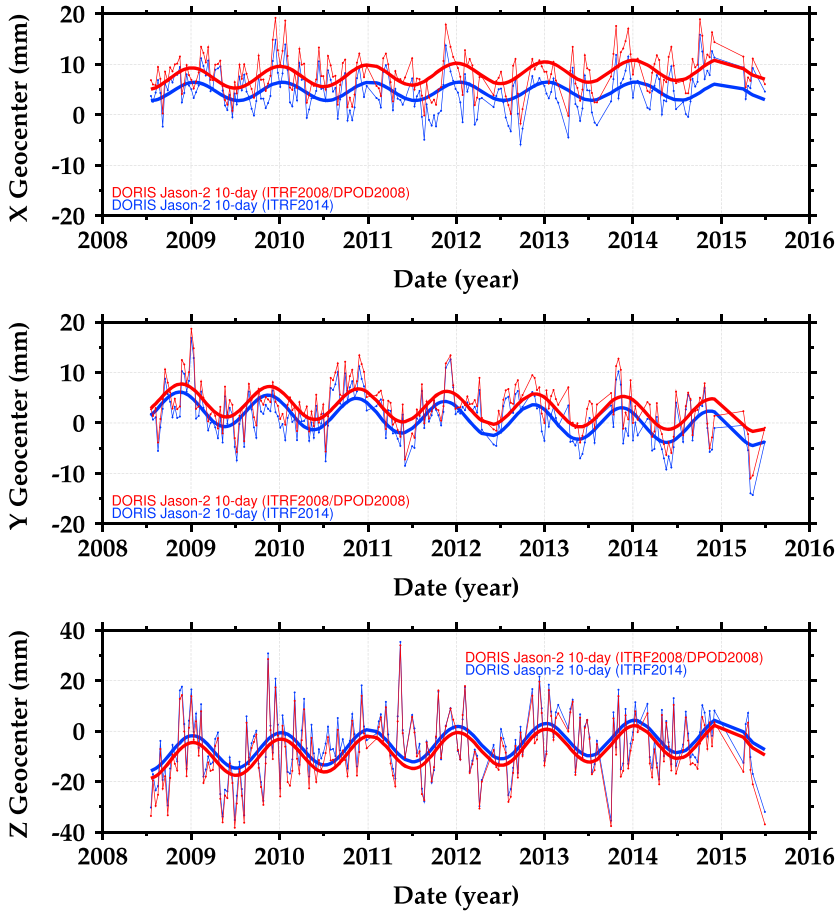

Figure 4. Ten-day estimates of DORIS-derived geocenter motion from Jason-2 GDR-E-like dynamic orbit series (July 2008 to June 2015; cycles 1–257), using the ITRF2008/DPOD2008 (red) and ITRF2014 (blue) coordinates for the DORIS stations. The solid curves are the results of the least squares fit to the geocenter variations of a bias, drift, and annual periods. DORIS = Doppler Orbitography and Radiopositioning Integrated by Satellite; ITRF = International Terrestrial Reference Frame; GDR = Geophysical Data Records.

Table 5
Effect of Switching From ITRF2008/DPOD2008 to ITRF2014 on the Annual Components of the Geocenter Motion of the DORIS-Derived Geocenter Motion From Jason-2

Solution	*A* ratio	$\delta\phi$ (day)
ITRF		
DX	0.9	11
DY	1.0	7
DZ	1.0	−1

Note. *A* ratio = amplitude ratio; $\delta\phi$ = phase shift; DORIS = Doppler Orbitography and Radiopositioning Integrated by Satellite.

of using the new terrestrial reference frame on altimeter satellite precise orbit determination. As a complement, we show in Figure 4 two DORIS-based geocenter time series relying on the ITRF2008/DPOD2008 and ITRF2014 realizations, to quantify the influence of errors contained in the older ITRF solution. Sites affected by major earthquakes, where the post seismic deformation (PSD) is accounted for in the ITRF2014 frame as detailed in Altamimi et al. (2016), are rejected. Only offsets and drifts can be seen between the two geocenter motion estimates (as confirmed by Figure 4 and Table 5), as is expected from the current ITRF solutions which assumes linear motions for ground stations (except for occasional discontinuities). Using ITRF2014 in place of ITRF2008/DPOD2008 reduces the geocenter coordinates systematic biases. This indicates that ITRF2014 represents an improvement over ITRF2008/DPOD2008 in this respect.

4.5. Subsequent Refinements

To improve annual and semiannual height variations determination, the tropospheric delay model GPT/GMF was replaced with the more accurate mapping functions VMF1 and the new empirical slant delay model GPT2 (Lagler et al., 2013). This model is an improved version of the existing models GPT/GMF and their replacement is recommended in the analysis of radio space geodetic observations for which seasonal variations are of interest.

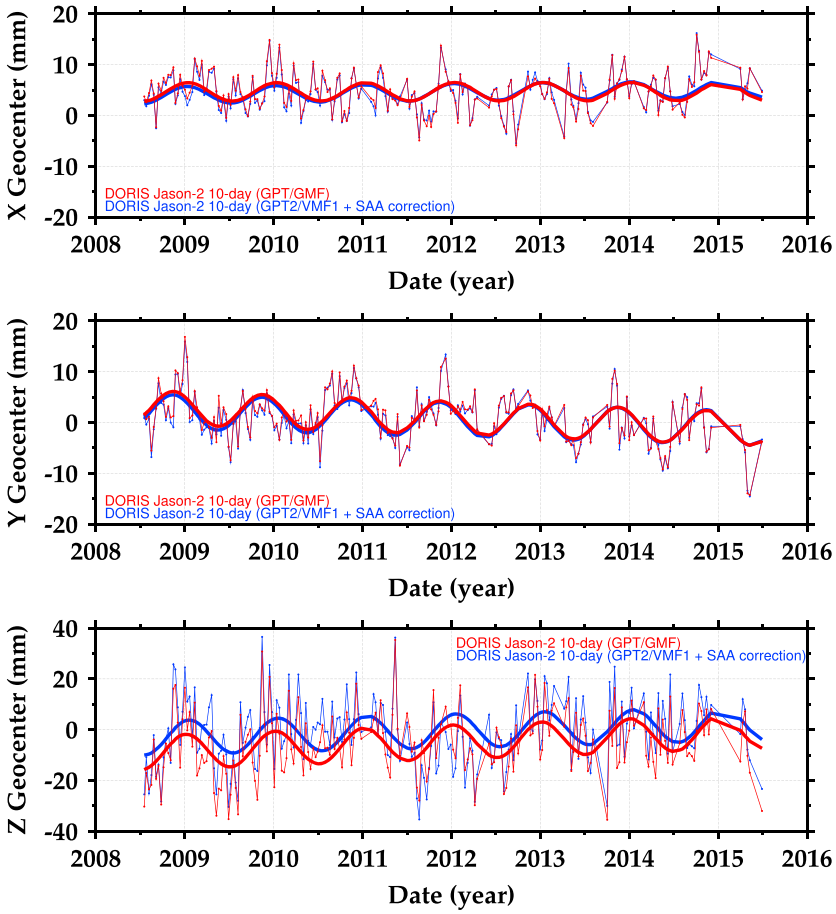

Figure 5. Ten-day estimates of DORIS-derived geocenter motion from Jason-2 GDR-E-like dynamic orbit series (July 2008 to June 2015; cycles 1–257), using the old tropospheric delay model GPT/GMF (red) and the new empirical model GPT2/VMF1 with the SAA effect corrected (blue). The solid curves are the results of the least squares fit to the geocenter variations of a bias, drift and annual periods. DORIS = Doppler Orbitography and Radiopositioning Integrated by Satellite; GDR = Geophysical Data Records; SAA = South Atlantic Anomaly; GPT = Global Pressure and Temperature; GMF = Global Mapping Function.

Table 6
Effect of Updating the Tropospheric Delay Model and Mitigating the South Atlantic Anomaly Perturbation on the Annual Components of the Geocenter Motion of the DORIS-Derived Geocenter Motion From Jason-2

Solution	*A* ratio	$\delta\phi$ (day)
Troposphere/SAA		
DX	0.9	−5
DY	1.0	−2
DZ	1.0	11

Note. *A* ratio = Amplitude ratio; $\delta\phi$ = Phase shift; DORIS = Doppler Orbitography and Radiopositioning Integrated by Satellite.

Figure 5 shows the consequences of this updated model for tropospheric correction on geocenter coordinates. In the blue solution, frequency drifts were also adjusted per pass for a set of selected DORIS sites located in the South Atlantic Anomaly (SAA) area: Arequipa, Peru; Ascension, United Kingdom (South Atlantic Ocean); Cachoeira-Paulista, Brazil; St-Helena, United Kingdom (South Atlantic Ocean); Kourou, France (French Guiana); Libreville, Gabon; and Sal, Cape Verde. Indeed, Willis et al. (2016) and Belli et al. (2016) observed in detail the sensitivity of the Jason-2 DORIS oscillator to radiations when the satellite passes over the SAA. This supplementary parameterization is able to mitigate well the spurious frequency drifts of the Jason-2 USO, manifesting as an offset in "SAA station" height estimates. As could have been anticipated, these final refinements mainly reflect on the Z geocenter coordinate, that is, removing a bias and slightly shifting the phase (Figure 5 and Table 6, respectively) of the seasonal signal.

At this last stage (see the blue solution of Figure 5), each of the preceding recommendations, identified in this analysis, has been taken in consideration when solving for geocenter motion with DORIS data. Table 7 summarizes the different strategies deployed in this study and the degree to which they contribute to the three geocenter coordinates at the annual frequency. The picture that emerges is that adjusting station heights and incorporating low-elevation DORIS data help by providing a better depiction of the motion of CF relative to CM, and as such act on the X component of the estimated annual geocenter motion. The improvement on the associated Z component is a result of the exclusive cross-track observability of the Z geocenter motion. Equation (10) also reveals the importance of SRP tuning for the axial component. Refining time-variable geopotential models, especially the atmospheric/oceanic gravitational dealiasing potentials, plays a significant role for the annual variations of the two equatorial geocenter motion components. The impact on geocenter motion estimates of using the new ITRF2014 realization is limited to offsets and drifts, as expected. Similarly, updating the tropospheric delay model and mitigating the SAA perturbation essentially remove a bias on the Z geocenter coordinate.

For validation purposes, the following subsection is devoted to comparing the optimal solution derived in this study against independent results.

4.6. Comparison to Independent Estimates

To validate our DORIS-based geocenter motion time series, we derived from the same Jason-2 satellite complementary SLR-based geocenter vector estimates (using the same monthly GRACE time series and ITRF2014 coordinates for the SLR stations). The dynamic parameterization strategy depicted in section 3 (one drag coefficient per arc, daily cross-track/along-track OPR accelerations, and empirical along-track constant accelerations estimated for every two orbital revolutions) is also used when computing SLR-only Jason-2 orbits. As demonstrated in subsection 4.2 through the analysis of the Hill equations, solving for SLR station biases and heights is necessary for not compromising the observability of the Z geocenter coordinate, while better sensing the motion of CF relative to CM (subsection 2.3). Figure 6 shows the effect of adjusting station heights and range biases (per station/arc, unconstrained) to mitigate vertical errors and secure an exclusive cross-track observability of the Z geocenter motion. This results in lower annual amplitude for the Z and especially for

Table 7
Sensitivity of the Mitigation Solutions on the Annual Components of the Geocenter Motion of the DORIS-Derived Geocenter Motion From Jason-2

Solution	*DX*	*DY*	*DZ*
Height adjustment	X		X
Low elevations	X		X
Draconitic			X
Geopotential	X	X	
ITRF			
Troposphere/SAA			(X)

Note. DORIS = Doppler Orbitography and Radiopositioning Integrated by Satellite; ITRF = International Terrestrial Reference Frame.

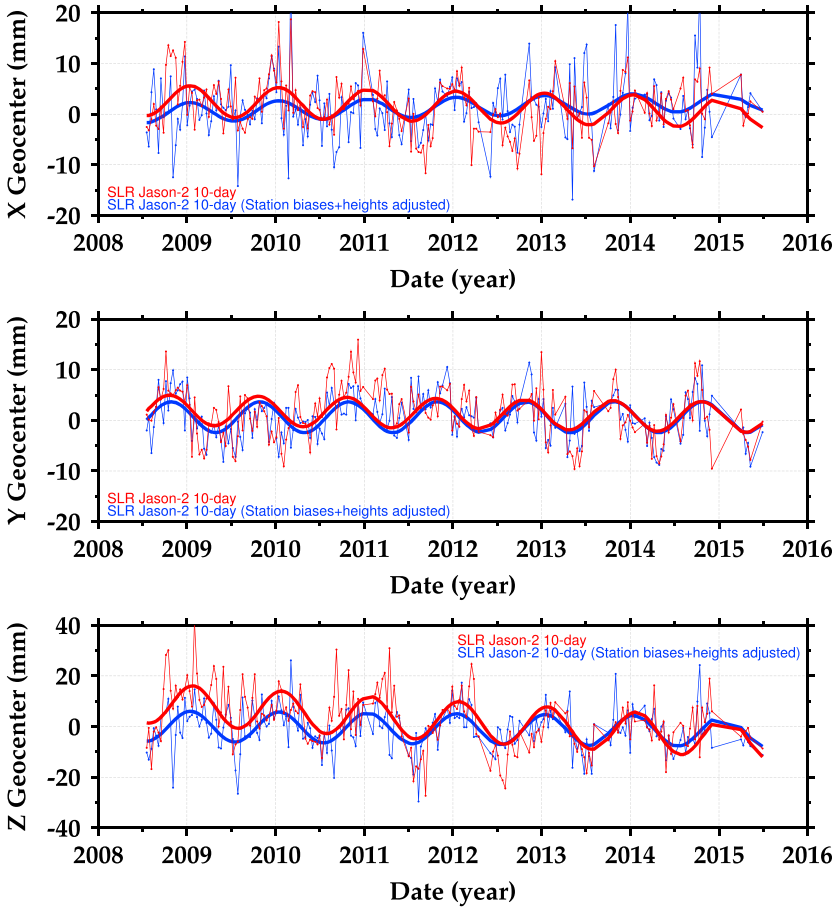

Figure 6. Ten-day estimates of SLR-derived geocenter motion from Jason-2 GDR-E-like dynamic orbit series (July 2008 to June 2015; cycles 1–257), with station biases and heights adjusted (blue) or not (red). The solid curves are the results of the least squares fit to the geocenter variations of a bias, drift and annual periods. SLR = Satellite Laser Ranging; GDR = Geophysical Data Records.

the X geocenter components (Table 8), and may explain why their variations in the SLR geocenter solutions are often overestimated in previously published results (Sośnica et al., 2013).

The very good agreement between the latter SLR Jason-2-based series and the associated DORIS-derived solution (compare the blue solutions displayed in Figure 5 and Figure 6) confirms the robustness of the two independent geodetic estimates. To facilitate a direct comparison of the geocenter coordinates derived from these two different Jason-2 solution types, the amplitudes and phases of the annual signals in the three Cartesian components are listed in Table 9 for each solution.

Table 8
Effect of Adjusting Station Heights and Biases on the Annual Components of the Geocenter Motion of the Satellite Laser Ranging-Derived Geocenter Motion From Jason-2

Solution	*A* ratio	$\delta\phi$ (day)
Bias/Height		
DX	0.6	0
DY	1.0	6
DZ	0.8	−10

Note. *A* ratio = Amplitude ratio; $\delta\phi$ = Phase shift.

Table 9
Estimates of Geocenter Annual Variations From This Study and Independent Results

	X		Y		Z	
Solution	A (mm)	ϕ (day)	A (mm)	ϕ (day)	A (mm)	ϕ (day)
GPS+GRACE	0.9	105	3.5	334	—	—
SLR L1+L2 (CN)	2.3	61	2.3	317	6.1	41
SLR L1+L2 (CF)	1.7	59	2.7	322	3.6	39
DORIS Jason-2	1.6	13	3.2	322	6.4	18
SLR Jason-2	1.5	21	3.1	302	5.9	21

Note. A ratio = Amplitude ratio; $\delta\phi$ = Phase shift; GPS = Global Positioning System; DORIS = Doppler Orbitography and Radiopositioning Integrated by Satellite; SLR = Satellite Laser Ranging; CN = center-of-network; CF = center-of-figure.

Comparisons from this study and published results of other studies are also performed and presented in Table 9 and Figure 7. The GPS+GRACE solution (3-day estimates) comes from Haines et al. (2015). For its Z component, the estimated annual geocenter motion should be disregarded because of spurious signals at the GRACE draconitic period (~ 320 days). The two SLR Laser Geodynamics Satellite (LAGEOS)-1 and 2 solutions (30-day estimates) are provided by Ries (2016). The CN monthly geocenter motion time series is consistent with the definition of the ITRF2014 origin. In the "CF" monthly solution, range biases were estimated for all SLR stations with a "relatively tight" a priori constraint. This approach has similarities with the one advocated in this study, except that we demonstrated in subsection 4.2 the necessity to also solve for station heights (DORIS and SLR solutions) without any constraint.

The three independent solutions (GPS + GRACE, SLR L1 + L2 ("CF"), DORIS Jason-2) corroborates to better than 1 mm, the smaller annual geocenter motion (0.9-1.7 mm) along the X axis (despite the uncertainty on the phase due to the small magnitude of the seasonal oscillations), and higher amplitude (2.7 − 3.5 mm) along

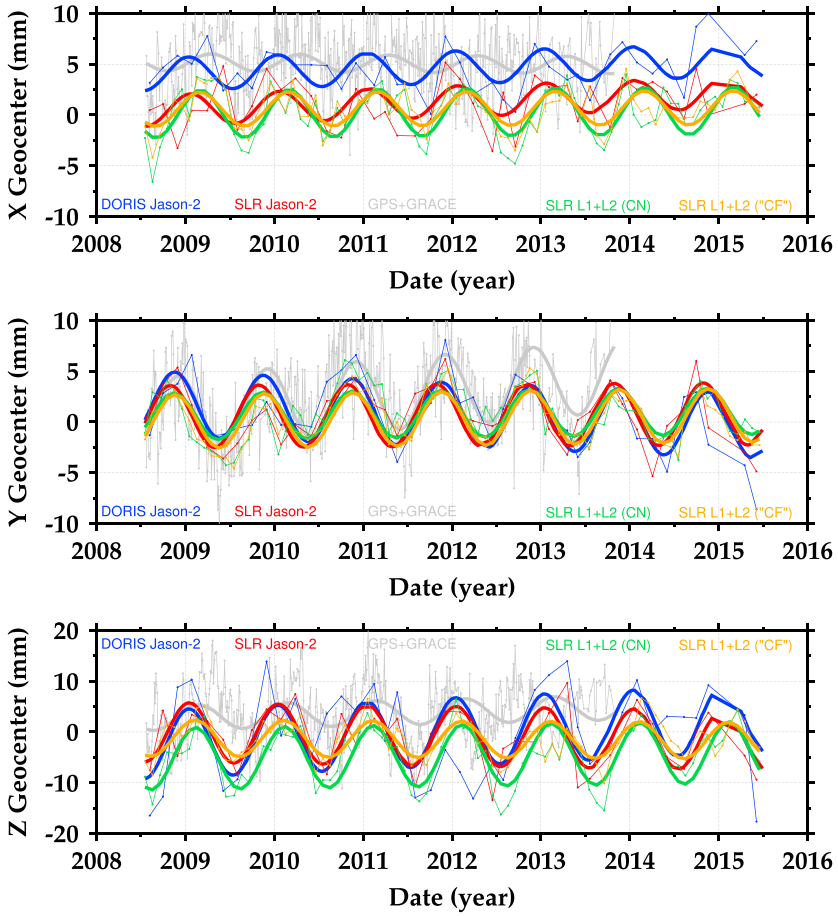

Figure 7. Three-day estimates of GPS + GRACE (Haines et al., 2015; gray), 30-day estimates of SLR LAGEOS-1 and 2 (Ries, 2016) CN (green) and "CF" (orange), 10-day estimates of DORIS (blue) and SLR (red) Jason-2 geocenter coordinates (this study) sampled at 60-day epochs for clarity. The solid curves are the results of the least squares fit to the geocenter variations of a bias, drift, and annual periods. DORID = Doppler Orbitography and Radiopositioning Integrated by Satellite; GPS = Global Positioning System; GRACE = Gravity Recovery and Climate Experiment; SLR = Satellite Laser Ranging; LAGEOS = Laser Geodynamics Satellite; CN = center-of-network; CF = center-of-figure.

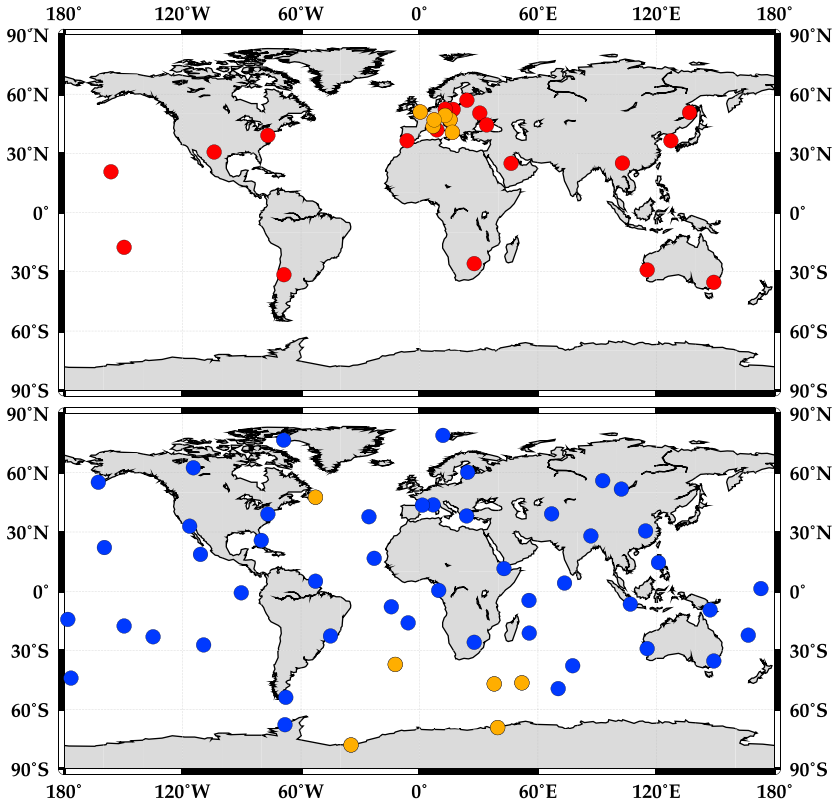

Figure 8. Ground network distribution of SLR (top) and DORIS (bottom) stations used in this study. Stations denoted with orange disks were removed to investigate network effects. SLR = Satellite Laser Ranging; DORIS = Doppler Orbitography and Radiopositioning Integrated by Satellite.

the Y axis. However, the Z annual amplitude is ∼ 4 mm with LAGEOS-only, whereas the DORIS/SLR-derived Jason-2 solutions from this study have a larger amplitude of ∼ 6 mm (cf. Table 9). There is also a systematic positive bias of ∼ 5 mm between the DORIS/GPS-derived and SLR-based geocenter motion estimates along the X axis (Figure 7, upper plot). Both observations are explained away in the following subsection.

4.7. Disentangling Uncertainties in the Realization of the ITRF Origin

The network distribution of SLR stations is not as well balanced as for DORIS or GNSS, with most of the high performing stations close to the X axis in the Norther Hemisphere (cf. Figure 8). Also, of the total number of SLR stations, on the order of only 12–15 are substantial contributors of data (e.g., see global performance report card for the SLR network available at https://ilrs.cddis.eosdis.nasa.gov/network/system_performance/global_report_cards). As noted in Collilieux et al. (2009), this implies a higher sensitivity of the X and Z geocenter coordinate estimates to network effects, because of the suboptimal geographic distribution of SLR stations. This is particularly true for the SLR-based X geocenter motion time series derived in this study, which experience a higher scatter than the Y component (see the blue solution of Figure 6). In contrast, the DORIS and GPS networks are to a great extent well balanced. As a consequence, their expected lower sensitivity to network effects may explain the better agreement between the DORIS Jason-2 and GPS + GRACE X geocenter motion estimates (Figure 7, upper plot).

Difficulties exist in ascertaining wether the poor geometry of the SLR network can explain the ∼ 5 mm SLR-based geocenter offs et along the X axis with respect to independent DORIS (and GPS) estimates. Indeed, the number of SLR stations colocated with DORIS sites is extremly small, making it impossible to solve for DORIS- and SLR-only geocenter coordinates over a common set of stations. Moreover, not all SLR stations are permanently available, which leads to a changeable (time-varying) configuration of the network and number of SLR tracking measurements from one station to another. To assess the SLR network effect on X geocenter estimates, we decided to artificially improve and degrade geometry of the SLR and DORIS stations, respectively, by removing stations near the Greenwich meridian and in the high-latitude area (i.e., where the stations

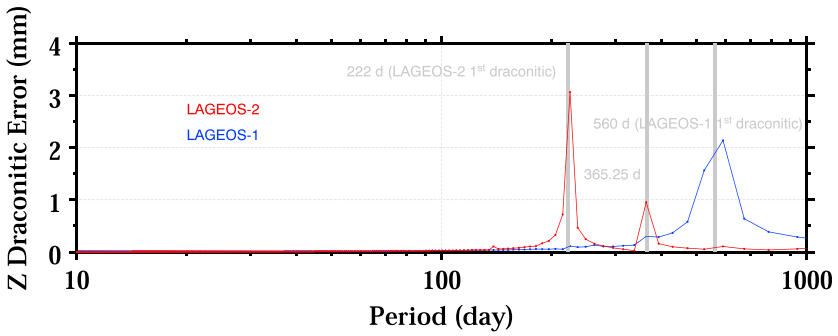

Figure 9. Amplitude spectra of estimated aliasing of LAGEOS-1 (blue) and 2 (red) draconitic errors into the Z geocenter coordinate derived from the Beta-prime angle evolution of the two satellites and equation (11). LAGEOS = Laser Geodynamics Satellite.

influence the determination of the X geocenter coordinate, since the visibility of Low Earth Orbiters strongly depends on their inclination angles). To this end, the most prolific European SLR stations in terms of data yield for the Jason-2 satellite (Zimmerwald, Switzerland; Herstmonceux, United-Kingdom; Graz, Austria; Grasse, France; Wettzell, Germany and Matera, Italy) and the following DORIS stations—to mimic the high concentration of SLR sites over Europe—(Crozet, France; Tristan-Da-Cunha, United-Kingdom (South Atlantic Ocean); Syowa, Antartica (Japanese base); St-John's, Canada; Marion-Island, South Africa; Belgrano, Antartica (Argentine base)) were subtracted. The orange disks in Figure 8 mark the stations removed for the analysis. This results in higher (1.2 mm ⇒ 2.4 mm) and lower (4.6 mm ⇒ 2.7 mm) SLR and DORIS X geocenter coordinate bias, respectively; hence canceling the systematic offset between the two solutions, when bridging the gap between the two networks. These findings corroborate the simulation study of Otsubo et al. (2016) indicating that additional SLR sites in the southern high latitudes would benefit the X geocenter component.

In this study, efforts have been made to minimize draconitic orbital perturbations in our geocenter motion estimates, making the most of the Jason-2 draconitic period (∼ 118 days), which can be well separated from one solar year (associated with the seasonal component of geophysical interest). The ITRF origin is only sensed by SLR observations of the LAGEOS-1 and 2 satellites. Assuming deficiencies in their SRP modeling at the level of 10$\c{p}$*percnt*;, a lower bound (provided that station heights and range biases are solved for, as recommended in subsection 4.2, or else the error would increase further) of the contamination of the LAGEOS draconitic errors in the Z geocenter motion time series can be described, analogously to equation (10), via the formula

$$Z_{\mathrm{Draconitic_{Error}}} \simeq -10\% \times 4 \times 10^{-9} \frac{r^3 \sin\beta}{GM \cos i}, \tag{11}$$

where β is the Beta-prime angle—Sun elevation angle over the orbital planes—of LAGEOS-1 and LAGEOS-2; and 4×10^{-9} is the amplitude of the acceleration (in m/s^2) due to direct SRP for the two satellites. Based on equation (11), the amplitude of the aliasing of LAGEOS-1 and 2 draconitic errors into the Z geocenter component is estimated at about 1 mm at the annual frequency, as can be seen in Figure 9.

The Yarkovsky-Schach thermal effect, affecting spinning satellites essentially along their spin axis, should be modeled when analyzing LAGEOS orbits. This perturbation is usually not modeled in orbit determination programs since the evolution of the satellite spin axis is not precisely known as well as its amplitude itself (59 pm/s^2, Afonso et al., 1989; 89.4 pm/s^2, Scharroo et al., 1991; 105 pm/s^2, Slabinski, 1996; and 241 pm/s^2, Métris et al., 1997, …). Given this lack of knowledge, we calculated an updated estimate of the Yarkovsky-Schach amplitude. As this perturbing acceleration mainly acts along the spin axis of the satellites (i.e., towards a specific inertial direction), we solved for two orthogonal accelerations along inertial directions in the equatorial plan of the Earth for the LAGEOS-1 and 2 satellites (the out-of-plan behavior of this acceleration cannot be estimated simultaneously as it is collinear with the axial geocenter motion). The obtained results are displayed in Figure 10. Focusing on the pre-2000 era, where the analyses of Andrés et al. (2004) and Kucharski et al. (2013) confirm a spin axis oriented essentially in the Z inertial direction for LAGEOS-1 (declination around −70°) and LAGEOS-2 (declination around −80°), we determined the value of the full Yarkovsky-Schach effect amplitude of the two satellites to be ∼ 600 pm/s^2, based on the previous equato-

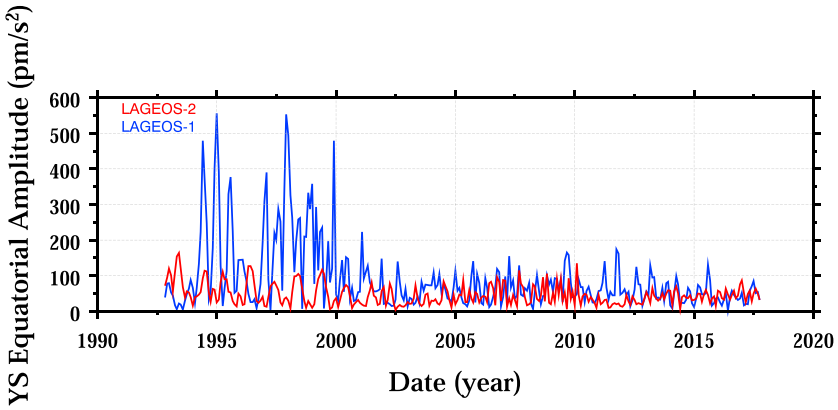

Figure 10. LAGEOS-1 (blue) and 2 (red) amplitudes of their inertial (Yarkovsky-Schach) equatorial perturbing accelerations. LAGEOS = Laser Geodynamics Satellite.

rial amplitude estimates of Figure 10 ($\sim$ 200 and $\sim$ 100pm/s^2, for LAGEOS-1 and 2, respectively) and their declination angles. This empirical finding is more than twice as large as given in Métris et al. (1997).

An estimate of the associated annual cross-track perturbation corrupting the Z geocenter coordinate can be derived from equation (10)

$$Z_{\text{Y-S}_{\text{Annual Error}}} \simeq -6 \times 10^{-10} \frac{r^3}{GM}, \tag{12}$$

where 6×10^{-10} is the amplitude of our estimate of the Yarkovsky-Schach acceleration, in m/s^2) for LAGEOS-1 and 2. Thus, not modeling the Yarkovsky-Schach effect can cause Z annual geocenter perturbations in LAGEOS-only geocenter motion time series of approximately 3 mm. The annual variations, already observed in Figure 10, have to do with the "seasons," that is, the tilt of the satellites' spin plan (close to the Earth's equator here) with respect to the ecliptic. This Z annual perturbation of $\sim$ 3 mm will thus conspire to decrease the amplitude of the geocenter motion, as the Yarkovsky-Schach force is directed away from the heated pole of the satellite (mind the minus sign of equation (12)). From the years 2000 onwards, the spin axes of the LAGEOS satellites both appear to follow a more complex evolution pattern (Andrés et al., 2004; Kucharski et al., 2013) and their complete modeling would be required to precisely derive the annual perturbation corrupting the LAGEOS-only Z geocenter coordinate.

The coupling of both error sources of nongravitational annual perturbations (SRP mismodelling and especially Yarkovsky-Schach thermal effect) for the orbits of LAGEOS-1 and 2 can definitely explain the 2 mm lower Z annual amplitude with LAGEOS-only than in the DORIS/SLR-derived Jason-2 solutions from this study. Indeed, when incorporating LARES data (the least perturbed LEO target by nonconservative forces and thermal effects) alongside LAGEOS-1 and 2 observations, Spatar (2016) also observed a 2-mm increase

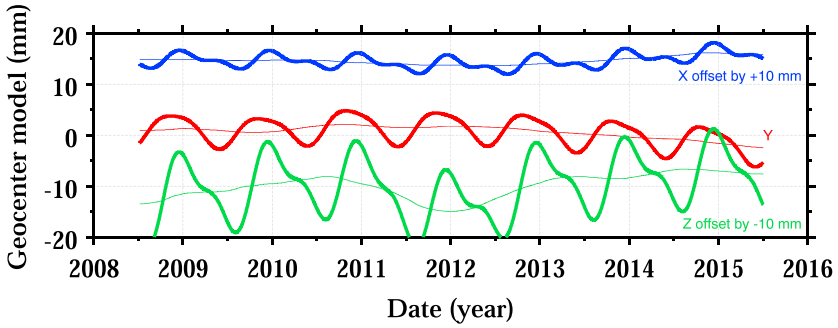

Figure 11. Smoothed DORIS-only Jason-2 geocenter motion time series using a Kalman filter. The bold lines represent the adjusted seasonal (semiannual and annual) and bias parameters, while the thin lines indicate the long-term component. Fictitious +10 and −10 mm offsets were introduced along the X and Z axes, respectively. DORIS = Doppler Orbitography and Radiopositioning Integrated by Satellite.

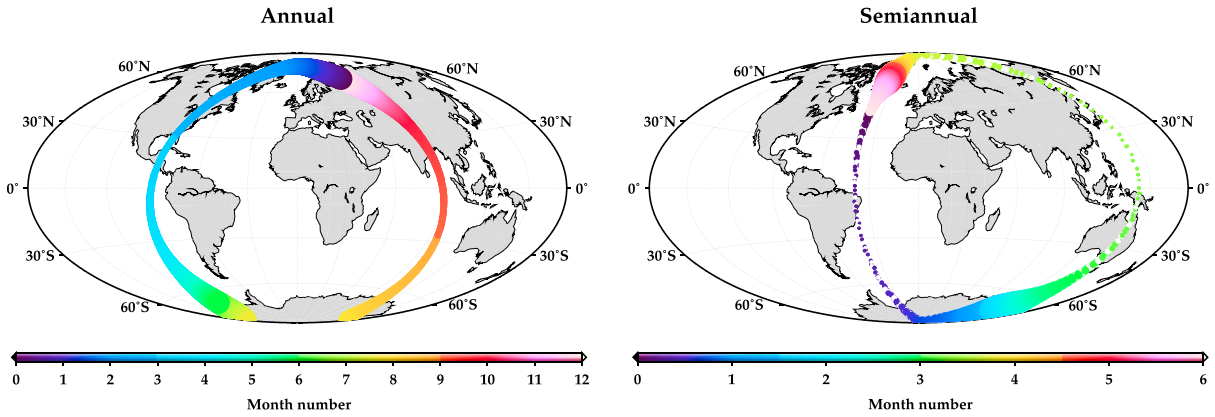

Figure 12. Annual (left) and semiannual (right) trajectories of the DORIS-only Jason-2 geocenter vector projected on the Earth's surface. Their magnitude (illustrated by the size of the colored dots) oscillates between 2–7 and 0–3 mm, for the annual and semiannual components, respectively. DORIS = Doppler Orbitography and Radiopositioning Integrated by Satellite.

in the amplitude of the annual signal in the Z geocenter vector component, while diminishing the aliasing of LAGEOS-specific errors.

4.8. Synthesis

As pointed out in Métivier et al. (2010), at the present-day, even if space geodesy geocenter estimates have proved their sensitivity to seasonal variations, we do not know exactly what kind of inter-annual geocenter motion one could expect to observe today in the context of climate change. Thus, forward modeling of the full nontidal (not only seasonal) geocenter motion is even more important nowadays for regional MSL studies. With that in mind, having an accepted model for altimeter satellite POD becomes especially a prerequisite for producing consistency between GPS-based and DORIS/SLR-derived orbits. Hence, a geocenter motion model was derived from our DORIS Jason-2-based time series to allow the investigation of seasonal and long-term variations. Figure 11 shows the model obtained which estimates bias, annual and semiannual sine and cosine parameters using a Kalman filter. The semiannual contribution is small compared to the annual component which seems to capture the main seasonal effects. Semiannual variations are essentially detectable in the X and Z geocenter vector components. The Z geocenter coordinate exhibits the strongest inter-annual variability. In particular, the north-south excursion over the period 2011–2012 could be attributed to Greenland's record melt (McMillan et al., 2016) and the exceptional persistence of Australian mass anomalies (Fasullo et al., 2013).

Figure 12 shows how the seasonal part of the geocenter motion model orientates when projected on the Earth's surface. An interesting feature concerns the strong elliptical polarisation of these trajectories, similar to what was observed by Bizouard (2016) with the hydro-atmospheric mass redistributions: The annual and semiannual components evolve in the great meridian circles of longitude $\sim$ 90° East and $\sim$ 150° East, respectively. By decomposing the annual and semiannual geocenter motions in the form $U_1 \cos(\omega t + \phi) + U_2 \sin(\omega t + \phi)$, with U_1 and U_2 orthogonal vectors given in mm and ϕ in days, it makes clear that the annual and semi annual geocenter motion signals lie in ellipses of parameters $[1.32.26.8]\cos(\omega t - 4) + [0.1 - 2.20.7]\sin(\omega t - 4)$ and $[0.8 - 0.72.8]\cos(2\omega t + 73) + [0.3 - 0.3 - 0.1]\sin(2\omega t + 73)$, respectively. Both ellipses are essentially oriented towards the north-south direction, especially the semiannual signal which has a very low semiminor-to-semimajor axis ratio of $\sim$ 15$\varsigma percnt$; ($\sim$ 30$\varsigma percnt$; for the annual signal). Annual variations surround the main continental regions of active terrestrial hydrological processes. Half-yearly variations are coherent and in phase with reported atmospheric pressure semiannual oscillations over northern Greenland and East Antarctica in Chen et al. (2012, their Figure 3). Understanding the physical sources of the full spectrum of geocenter variations should be a major goal in the future analysis.

5. Conclusions

To elucidate how model and geodetic technique errors propagate into the ITRF origin, we have examined independently derived geocenter motion time series using DORIS observations from the OSTM/Jason-2 satel-

lite over the period 2008.5–2015.5. The analysis identified dominant sources of correlations and modeling issues, which should be mitigated when estimating the geocenter coordinates.

Overall, our results show that the Jason-2 satellite is particularly appealing for geodetic geocenter motion determination since it fulfills the useful conditions of having an inclination much below 90° (unlike the sun-synchronous satellites), a draconitic period not close to one solar year (in contrast to the GPS satellites), a well known inertial attitude (differently from the spinning LAGEOS satellites) and a high sensitivity to geocenter motion (with an altitude close to the optimal LEO target LARES). Based on the TOPEX/Poseidon and Jason-1 legacy missions, initiating an independent geocenter time series in 1992 is also possible. Even if it is currently not possible to benefit from combining other satellites (most altimeter missions are sun-synchronous) with Jason-2 for DORIS-based geocenter motion estimates, the upcoming consecutive launches of HY-2C (inclination of 66°), Jason-CS/Sentinel-6, and SWOT (inclination of 78°; draconitic period of 78.5 days) will make possible a combination in the future.

The DORIS-derived geocenter motion time series presented here are in very good agreement in both annual amplitude and phase with SLR observations also based on Jason-2. The systematic $\sim$ 5mm offset along the X axis between the two geodetic estimates of geocenter motion has been attributed to the unbalanced SLR network. These results are also consistent at the level of 1 mm with independent GPS + GRACE and SLR + LAGEOS solutions, for the annual variations of the two equatorial geocenter motion components. However, unlike what was derived in earlier studies based on LAGEOS-only SLR observations, the estimated amplitude of the annual signal in the axial direction is found here to be $\sim$ 2mm higher (6.0–6.5mm). The genuine differences between this analysis and past results originate from the rigorous treatment of correlations proposed in this study when estimating geocenter coordinates:

1. the adjustment of station heights (and biases for SLR stations) without constraints,
2. the inclusion of low-elevation DORIS data,
3. the identification and reduction of aliased draconitic signatures into the annual sinusoidal Z geocenter coordinate, and
4. the use of state-of-the-art models (gravity and troposphere modeling).

The analysis presented here reveals that SLR geocenter solutions (from Jason-2 but also LAGEOS) are sensitive to station heights modeling errors, making their estimation necessary (as well as station biases). Unfortunately, for LAGEOS-only solutions, the contribution of the Yarkovsky-Schach perturbation is not negligible (estimated of 2–3mm for the Z coordinate). The traditional CN approach does not suffer from this problem, but still may not be fully consistent with the CF estimates due to network effects. Even with less observability per pass for the DORIS technique, its large and homogeneous network should allow a better realization for CF.

Acknowledgments
A. Couhert gratefully acknowledges support by the Centre National d'Etudes Spatiales and Groupe de Recherche de Géodésie Spatiale. This work takes advantage of the IDS (Willis et al., 2010) and ILRS data (Pearlman et al., 2002). The DORIS and SLR tracking data over the low-Earth Jason-2/OSTM satellite are available from ftp://ftp.cddis.eosdis.nasa.gov/pub/doris/data/ja2 and ftp://cddis.gsfc.nasa.gov/pub/slr/data/npt_crd/jason2, respectively.

References

Afonso, G., Barlier, F., Mignard, F., Carpino, M., & Farinella, P. (1989). Orbital effects of LAGEOS seasons and eclipses. *Annales Geophysicae*, *7*, 501–514.

Altamimi, Z., Collilieux, X., & Métivier, L. (2011). ITRF2008: An improved solution of the international terrestrial reference frame. *Journal of Geodesy*, *85*(8), 457–473. https://doi.org/10.1007/s00190-011-0444-4

Altamimi, Z., Rebischung, P., Métivier, L., & Collilieux, X. (2016). ITRF2014: A new release of the International Terrestrial Reference Frame modeling nonlinear station motions. *Journal of Geophysical Research: Solid Earth*, *121*, 6109–6131. https://doi.org/10.1002/2016JB013098

Andrés, J. I., Noomen, R., Bianco, G., Currie, D. G., & Otsubo, T. (2004). Spin axis behavior of the LAGEOS satellites. *Journal of Geophysical Research*, *109*, B06403. https://doi.org/10.1029/2003JB002692

Beckley, B. D., Lemoine, F. G., Luthcke, S. B., Ray, R. D., & Zelensky, N. P. (2007). A reassessment of global and regional mean sea level trends from TOPEX and Jason-1 altimetry based on revised reference frame and orbits. *Geophysical Research Letters*, *34*, L14608. https://doi.org/10.1029/2007GL030002

Belli, A., Exertier, P., Samain, E., Courde, C., Vernotte, F., Jayles, C., & Auriol, A. (2016). Temperature, radiation and aging analysis of the DORIS Ultra Stable Oscillator by means of the Time Transfer by Laser Link experiment on Jason-2. *Advances in Space Research*, *58*(12), 2589–2600. https://doi.org/10.1016/j.asr.2015.11.025

Bizouard, C. (2016). Elliptic polarisation of the polar motion excitation. *Journal of Geodesy*, *90*(2), 179–188. https://doi.org/10.1007/s00190-015-0864-7

Blewitt, G. (2003). Self-consistency in reference frames, geocenter definition, and surface loading of the solid Earth. *Journal of Geophysical Research*, *108*(B2), 2103. https://doi.org/10.1029/2002JB002082

Blewitt, G., Lavallée, D., Clarke, P., & Nurutdinov, K. (2001). A new global mode of Earth deformation: Seasonal cycle detected. *Science*, *294*(5550), 2342–2345. https://doi.org/10.1126/science.1065328

Boehm, J., Heinkelmann, R., & Schuh, H. (2007). Short note: A global model of pressure and temperature for geodetic applications. *Journal of Geodesy*, *81*(10), 679–683. https://doi.org/10.1007/s00190-007-0135-3

Boehm, J., Niell, A., Tregoning, P., & Schuh, H. (2006). Global Mapping Function (GMF): A new empirical mapping function based on numerical weather model data. *Geophysical Research Letters*, *33*, l07304. https://doi.org/10.1029/2005GL025546

Boehm, J., Werl, B., & Schuh, H. (2006). Troposphere mapping functions for GPS and very long baseline interferometry from European Centre for Medium-Range Weather Forecasts operational analysis data. *Journal of Geophysical Research*, *111*, B02406. https://doi.org/10.1029/2005JB003629

Böhm, J., Schuh, H., & Weber, R. (2002). Influence of tropospheric zenith delays obtained by GPS and VLBI on station heights. In H. Drewes, et al. (Eds.), *Vertical Reference Systems* (pp. 107–112). Berlin, Heidelberg: Springer.

Chanard, K., Fleitout, L., Calais, E., Rebischung, P., & Avouac, J.-P. (2018). Toward a global horizontal and vertical elastic load deformation model derived from GRACE and GNSS station position time series. *Journal of Geophysical Research: Solid Earth*, *123*, 3225–3237. https://doi.org/10.1002/2017JB015245

Chen, G., Qian, C., & Zhang, C. (2012). New insights into annual and semiannual cycles of sea level pressure. *Monthly Weather Review*, *140*(4), 1347–1355. https://doi.org/10.1175/MWR-D-11-00187.1

Cheng, M. K., Ries, J. C., & Tapley, B. D. (2013). *Geocenter variations from analysis of SLR data* (pp. 19–25). Berlin, Heidelberg: Springer. https://doi.org/10.1007/978-3-642-32998-2

Collilieux, X., Altamimi, Z., Ray, J., van Dam, T., & Wu, X. (2009). Effect of the Satellite Laser Ranging network distribution on geocenter motion estimation. *Journal of Geophysical Research*, *114*, B04402. https://doi.org/10.1029/2008JB005727

Couhert, A., Cerri, L., Legeais, J.-F., Ablain, M., Zelensky, N. P., Haines, B. J., et al. (2015). Towards the 1 mm/y stability of the radial orbit error at regional scales. *Advances in Space Research*, *55*(1), 2–23. https://doi.org10.1016/j.asr.2014.06.041

Crétaux, J.-F., Soudarin, L., Davidson, F. J. M., Gennero, M.-C., Bergé-Nguyen, M., & Cazenave, A. (2002). Seasonal and interannual geocenter motion from SLR and DORIS measurements: Comparison with surface loading data. *Journal of Geophysical Research*, *107*(B12), 2374. https://doi.org/10.1029/2002JB001820

Davies, P., & Blewitt, G. (2000). Methodology for global geodetic time series estimation: A new tool for geodynamics. *Journal of Geophysical Research*, *105*(B5), 11,083–11,100. https://doi.org/10.1029/2000JB900004

Dong, D., Dickey, J. O., Chao, Y., & Cheng, M. K. (1997). Geocenter variations caused by atmosphere, ocean and surface ground water. *Geophysical Research Letters*, *24*(15), 1867–1870. https://doi.org/10.1029/97GL01849

Dong, D., Qu, W., Fang, P., & Peng, D. (2014). Non-linearity of geocentre motion and its impact on the origin of the terrestrial reference frame. *Geophysical Journal International*, *198*(2), 1071. https://doi.org/10.1093/gji/ggu187

Dong, D., Yunck, T., & Heflin, M. (2003). Origin of the International Terrestrial Reference Frame. *Journal of Geophysical Research*, *108*(B4), 2200. https://doi.org/10.1029/2002JB002035

Dumont, J. P., Rosmorduc, V., Carrere, L., Picot, N., Bronner, E., Couhert, A., et al. (2017). OSTM/Jason-2 Products Handbook (Issue 1, rev 11, pp. 33–35). Retrieved from https://www.aviso.altimetry.fr/fileadmin/documents/data/tools/hdbk_j2.pdf

Fasullo, J. T., Boening, C., Landerer, F. W., & Nerem, R. S. (2013). Australia's unique influence on global sea level in 2010-2011. *Geophysical Research Letters*, *40*, 4368–4373. https://doi.org/10.1002/grl.50834

Gobinddass, M. L., Willis, P., de Viron, O., Sibthorpe, A., Zelensky, N. P., Ries, J. C., et al. (2009). Systematic biases in DORIS-derived geocenter time series related to solar radiation pressure mis-modeling. *Journal of Geodesy*, *83*(9), 849–858. https://doi.org/10.1007/s00190-009-0303-8

Gobinddass, M., Willis, P., de Viron, O., Sibthorpe, A., Zelensky, N. P., Ries, J., et al. (2009). Improving {DORIS} geocenter time series using an empirical rescaling of solar radiation pressure models. *Advances in Space Research*, *44*(11), 1279–1287. https://doi.org/10.1016/j.asr.2009.08.004

Haines, B. J., Bar-Sever, Y. E., Bertiger, W. I., Desai, S. D., Harvey, N., Sibois, A. E., & Weiss, J. P. (2015). Realizing a terrestrial reference frame using the Global Positioning System. *Journal of Geophysical Research: Solid Earth*, *120*, 5911–5939. https://doi.org/10.1002/2015JB012225

Heflin, M., Bertiger, W., Blewitt, G., Freedman, A., Hurst, K., Lichten, S., et al. (1992). Global geodesy using GPS without fiducial sites. *Geophysical Research Letters*, *19*(2), 131–134. https://doi.org/10.1029/91GL02933

Kucharski, D., Lim, H.-C., Kirchner, G., & Hwang, J.-Y. (2013). Spin parameters of LAGEOS-1 and LAGEOS-2 spectrally determined from Satellite Laser Ranging data. *Advances in Space Research*, *52*(7), 1332–1338. https://doi.org/10.1016/j.asr.2013.07.007

Lagler, K., Schindelegger, M., Boehm, J., Krásná, H., & Nilsson, T. (2013). GPT2: Empirical slant delay model for radio space geodetic techniques. *Geophysical Research Letters*, *40*, 1069–1073. https://doi.org/10.1002/grl.50288

Lavallée, D. A., van Dam, T., Blewitt, G., & Clarke, P. J. (2006). Geocenter motions from GPS: A unified observation model. *Journal of Geophysical Research*, *111*, B05405. https://doi.org/10.1029/2005JB003784

McMillan, M., Leeson, A., Shepherd, A., Briggs, K., Armitage, T. W. K., Hogg, A., et al. (2016). A high-resolution record of Greenland mass balance. *Geophysical Research Letters*, *43*, 7002–7010. https://doi.org/10.1002/2016GL069666

Meindl, M., Beutler, G., Thaller, D., Dach, R., & Jäggi, A. (2013). Geocenter coordinates estimated from GNSS data as viewed by perturbation theory. *Advances in Space Research*, *51*(7), 1047–1064. https://doi.org/10.1016/j.asr.2012.10.026

Métivier, L., Greff-Lefftz, M., & Altamimi, Z. (2010). On secular geocenter motion: The impact of climate changes. *Earth and Planetary Science Letters*, *296*(3-4), 360–366. https://doi.org/10.1016/j.epsl.2010.05.021

Métris, G., Vokrouhlicky, D., Ries, J. C., & Eanes, R. J. (1997). Nongravitational effects and the LAGEOS eccentricity excitations. *Journal of Geophysical Research*, *102*(B2), 2711–2729. https://doi.org/10.1029/96JB03186

Morel, L., & Willis, P. (2005). Terrestrial reference frame effects on global sea level rise determination from TOPEX/Poseidon altimetric data. *Advances in Space Research*, *36*(3), 358–368. satellite Dynamics in the Era of Interdisciplinary Space Geodesy.

Otsubo, T., Matsuo, K., Aoyama, Y., Yamamoto, K., Hobiger, T., Kubo-oka, T., & Sekido, M. (2016). Effective expansion of Satellite Laser Ranging network to improve global geodetic parameters. *Earth, Planets and Space*, *68*(1), 65. https://doi.org/10.1186/s40623-016-0447-8

Pearlman, M. R., Degnan, J. J., & Bosworth, J. M. (2002). The International Laser Ranging Service. *Advances in Space Research*, *30*(2), 135–143. https://doi.org/10.1016/S0273-1177(02)00277-6

Petit, G., & Luzum, B. (2010). IERS Conventions (IERS Technical Note 36). Frankfurt, Germany: Verlag des Bundesamts für Kartographie und Geodäsie. Retrieved from https://www.iers.org/SharedDocs/Publikationen/EN/IERS/Publications/tn/TechnNote36/tn36.html

Ray, J. (1999). IERS analysis campaign to investigate motions of the geocenter (*IERS Technical Note, 25*). Paris: Observatoire de, Paris.

Ray, J., Altamimi, Z., Collilieux, X., & van Dam, T. (2008). Anomalous harmonics in the spectra of GPS position estimates. *GPS Solutions*, *12*(1), 55–64. https://doi.org/10.1007/s10291-007-0067-7

Riddell, A. R., King, M. A., Watson, C. S., Sun, Y., Riva, R. E. M., & Rietbroek, R. (2016). Uncertainty in geocenter estimates in the context of ITRF2014. *Journal of Geophysical Research: Solid Earth*, *122*, 4020–4032. https://doi.org/10.1002/2016JB013698

Ries, J. C. (2013). Seasonal geocenter motion from space geodesy and models. In *IERS Retreat 2013*. Paris, France. 23-24 May, 2013. Retrieved from https://www.iers.org/SharedDocs/Publikationen/EN/IERS/Workshops/Retreat2013/7_Ries.pdf?__blob=publicationFile&v=1

Ries, J. C. (2016). Reconciling estimates of annual geocenter motion from space geodesy (Tech. Rep) The University of Texas at Austin Center for Space Research, Texas, Austin, USA.

Rothacher, M. (2002). *Estimation of Station Heights with GPS* (pp. 81–90). Berlin, Heidelberg: Springer. https://doi.org/10.1007/978-3-662-04683-8

Scharroo, R., Waker, K. F., Ambrosius, B. A. C., & Noomen, R. (1991). On the along-track acceleration of the LAGEOS satellite. *Journal of Geophysical Research*, *96*(B1), 729–740. https://doi.org/10.1029/90JB02080

Slabinski, V. J. (1996). A numerical solution for LAGEOS thermal thrust: The rapid-spin case. *Celestial Mechanics and Dynamical Astronomy*, *66*(2), 131–179. https://doi.org/10.1007/BF00054962

Sośnica, K. (2015). Determination of precise satellite orbits and geodetic parameters using Satellite Laser Ranging (*Technical report, Geodätisch-geophysikalische Arbeiten in der Schweiz, 93*). Eidg. Technische Hochschule Zürich, Zürich: Schweizerische Geodätische Kommission, Institut for Geodäsie und Photogrammetrie.

Sośnica, K., Thaller, D., Dach, R., Jäggi, A., & Beutler, G. (2013). Impact of loading displacements on SLR-derived parameters and on the consistency between GNSS and SLR results. *Journal of Geodesy*, *87*(8), 751–769. https://doi.org/10.1007/s00190-013-0644-1

Spatar, C. B. (2016). Observability and estimation of geocentre motion using multi-Satellite Laser Ranging (PhD thesis), Newcastle University. https://doi.org/hdl.handle.net/10443/3333

Stammer, D., & Cazenave, A. (2018). *Satellite altimetry over oceans and land surfaces* (pp. 670). Boca Raton, FL: CRC Press.

Sun, Y., Ditmar, P., & Riva, R. (2017). Statistically optimal estimation of degree-1 and C20 coefficients based on GRACE data and an ocean bottom pressure model. *Geophysical Journal International*, *210*(3), 1305–1322. https://doi.org/10.1093/gji/ggx241

Swenson, S., Chambers, D., & Wahr, J. (2008). Estimating geocenter variations from a combination of GRACE and ocean model output. *Journal of Geophysical Research*, *113*, B08410. https://doi.org/10.1029/2007JB005338

Tregoning, P., & van Dam, T. (2005). Effects of atmospheric pressure loading and seven-parameter transformations on estimates of geocenter motion and station heights from space geodetic observations. *Journal of Geophysical Research*, *110*, B03408. https://doi.org/10.1029/2004JB003334

Willis, P., Berthias, J. P., & Bar-Server, Y. E. (2006). Systematic errors in the Z-geocenter derived using satellite tracking data: A case study from SPOT-4 DORIS data in 1998. *Journal of Geodesy*, *79*(10), 567–572. https://doi.org/10.1007/s00190-005-0013-9

Willis, P., Fagard, H., Ferrage, P., Lemoine, F. G., Noll, C. E., Noomen, R., et al. (2010). The International DORIS Service (IDS): Toward maturity. *Advances in Space Research*, *45*(12), 1408–1420. https://doi.org/10.1016/j.asr.2009.11.018

Willis, P., Heflin, M. B., Haines, B. J., Bar-Sever, Y. E., Bertiger, W. I., & Mandea, M. (2016). Is the Jason-2 DORIS oscillator also affected by the South Atlantic Anomaly? *Advances in Space Research*, *58*(12), 2617–2627. https://doi.org/10.1016/j.asr.2016.09.015

Wu, X., Kusche, J., & Landerer, F. W. (2017). A new unified approach to determine geocentre motion using space geodetic and grace gravity data. *Geophysical Journal International*, *209*(3), 1398–1402. https://doi.org/10.1093/gji/ggx086

Wu, X., Ray, J., & van Dam, T. (2012). Geocenter motion and its geodetic and geophysical implications. *Journal of Geodynamics*, *58*, 44–61. https://doi.org/10.1016/j.jog.2012.01.007

Zannat, U. J., & Tregoning, P. (2017). Estimating network effect in geocenter motion: Theory. *Journal of Geophysical Research: Solid Earth*, *122*, 8360–8375. https://doi.org/10.1002/2017JB014246

Zelensky, N. P., Lemoine, F. G., Beckley, B. D., Chinn, D. S., & Pavlis, D. E. (2018). Impact of ITRS 2014 realizations on altimeter satellite precise orbit determination. *Advances in Space Research*, *61*(1), 45–73. https://doi.org/10.1016/j.asr.2017.07.044